Optical and mechanical testing of 3D printed parts made of high-viscosity silicone to identify process parameters and design advice for 3D printing and printer development

Joel Schön, Robin Löffler ✉ and Michael Koch

Technische Hochschule Nürnberg Georg Simon Ohm, Germany

✉ robin.loeffler@th-nuernberg.de

Abstract

The additive manufacturing of parts made from close-to-production materials poses a great challenge. One example are highly viscous silicones, as used in injection moulding. For small production quantities, the manufacturing of injection moulds is uneconomical. This paper presents tensile specimens printed with an in-house developed dispensing system, which are analysed for air cavities (micro-CT scans) and mechanical properties. Based on the results, advice for the design and slicing parameters of parts using high-viscosity silicones in AM by means of material extrusion are developed.

Keywords: additive manufacturing, 3D printing, silicone, liquid rubber, process analysis

1. Introduction

1.1. Motivation

3D printing of silicones allows a cost-effective fabrication of flexible, soft and food safe parts. However, the variety of silicones, manufacturers of silicone-processing printers and description of relevant parameters for the design and preprint preparation (slicing) of parts is limited, especially for high-viscosity silicones from the injection moulding industry. For these silicones, AM offers an economical alternative, as prototypes and small batches can be produced more cost-effectively than with an injection moulding machine. The machining of injection moulds as well as the production of peripheral components is no longer necessary. In the AM of such silicone parts, it is important that the mechanical properties of the parts are as close as possible to those of the series product. These parts properties strongly depend on the bonding of the individually printed layers, which is why internal air cavities in the parts must be avoided. Based on this challenge, this paper examines tensile specimens (ISO 37 Type 1), made of high-viscosity silicone rubber (Elastosil LR 3003/50 A/B), using micro-computer tomography (micro-CT) scans and tensile tests. These specimens were manufactured on a custom-designed 3D printer, using different settings for preprint preparation and printing. The micro-CT scans provide information about possible air cavities in the uncured base material as well as about cavities within the tensile specimens due to the layered structure. The results of these scans are compared with tensile tests of the respective test specimens and examined for correlations. These results demonstrate that, using suitable process parameters, components made from industrial silicones, with comparable tensile strengths to injection-moulded samples, can be produced with the help of a low-cost 3D printer.

1.2. State of research

The following publications are available on the development of silicone processing 3D printers and the analysis of the process parameters used. Liravi et al. (2015) studied the influence of pressure, printing speed and layer height on the quality of the printed part. Two- and three-dimensional shapes are printed with a UV-curing silicone and examined for line width, uniformity and surface quality. The authors Martin et al. (2021) developed a low-cost silicone printer for medical applications. A piston extruder feeds two components synchronously through a mixing tube, at a viscosity of 1800 mPa·s. The results also present printing parameters such as printing speed, line width and layer height. Plott and Shih (2017) use one-component silicone, which is cured by humidity. Various experiments resulted in a flow rate and compression factor as well as other capabilities. The aim of the work was to reduce air cavities in the printed part. Luis et al. (2020) also uses a two-component silicone to produce meniscus implants. First, the rheology and the temperature-dependent curing time of two silicones were investigated. Subsequently, printing tests were carried out by changing the parameters printing speed, nozzle diameter, nozzle temperature and print bed temperature. Regarding the tensile strength of silicone rubber, there is a scientific publication by Leineweber et al. (2022). They print silicone rubber with a thermoplastic shell and investigate the relationship between tensile strength and curing time. The special feature is that a thermoplastic shell is printed at the same time as the tensile specimen, which prevents the silicone rubber from running. This makes it possible to vulcanize the entire tensile specimen after printing. Liu et al. (2023) are using carbon fiber as reinforcement of silicon composite structures. They compare tensile specimens with and without fiber reinforcement as well as the orientation of the printed silicone.

2. Materials and methods

2.1. Silicone specifications

Elastosil LR 3003/50 A/B (Wacker Chemie AG, Munich, Germany), is a liquid silicone rubber which cures after mixing components A and B using, for example, a static mixer. Both components are mixed in a ratio of 1:1. Table 1 contains the values for the dynamic viscosity of the liquid silicone. Both components of the silicone have the same viscosity. The high viscosity of the liquid silicone is the main difference to other silicones used currently in additive manufacturing. This silicone can be used for a wide range of applications, is mechanically as well as electrically very robust and also food safe.

Table 1. Technical data Elastosil LR 3003/50 A/B, uncured (Wacker Chemie AG, 2022)

Property	Value	Method
Viscosity, dynamic ($1\ s^{-1}$)	1100000 mPa·s	DIN EN ISO 3219
Viscosity, dynamic ($10\ s^{-1}$)	410000 mPa·s	DIN EN ISO 3219

Table 2 below describes the mechanical properties of the cured silicone. The most relevant values are the tensile strength and the maximum elongation at failure of the test specimen in order to be able to make a comparison with the 3D printed samples. For these tests on mechanical strength, test specimens punched from sheet material according to ISO 37 Type 1 are used. The geometry of the test specimens is described in chapter 2.4., as this shape is applied to the 3D printed specimens.

Table 2. Technical data Elastosil LR 3003/50 A/B, cured (Wacker Chemie AG, 2022)

Property	Value	Method
Hardness Shore A	50	DIN ISO 48-4
Density	1.13 g/cm³	DIN EN ISO 1183-1 A
Tensile strength	10.3 N/mm²	ISO 37 Type 1
Elongation at break	490 %	ISO 37 Type 1
Tear strength	26 N/mm	ASTM D 624 B

2.2. Silicone rheology

To supplement the manufacturer's data, our own preliminary rheological investigations were carried out during operation of the feeding system and with the use of a rheometer. Using pressure sensors at various positions in the feeding system, it was possible to identify a temperature-dependent behaviour of the silicone during the printing process. As the temperature increases, the viscosity decreases and vice versa. To determine the flow curve, the silicone was examined by means of a rotation measurement in a rheometer MCR301 (Anton Paar GmbH., Ostfildern-Scharnhausen, Germany). Elastosil exhibits a structurally viscous behaviour. With higher shear rate the viscosity decreases. Component A is also more viscous than component B. Furthermore, analogous to the measurements in the feeding system, a reduction in viscosity with increasing temperature is evident.

Also, the storage and loss modulus are analysed in relation to the angular frequency. In this measurement, one disc oscillates above a second disc. The silicone is located in between. The storage modulus indicates how much energy the material stores through elastic behaviour. The loss modulus is equivalent to dissipation. The material therefore deforms plastically.

2.3. Design of the feeding and printing system

A sketch of the entire system can be seen in Figure 1. It is assembled from a feeding unit and a modified FDM (fused deposition modeling) printer. The feeding unit has two 40 mm inner diameter cylinders into which the silicon components are filled. Two linear units move the push rods and pistons independently. The pistons push the two silicone components through high-pressure hoses with internal diameters of 10 mm to the mixing tower. This mixing tower serves as the interface between the two silicone components and the static mixer. The material is then fed to the print head through a PTFE hose with an inner diameter of 6 mm. The print head can be heated and realises the movements in x- and y-direction. Finally, the silicone is applied with a 0.84 mm dispensing needle to the print bed.

Since the hose sections of the silicone supply, starting from the cylinders up to the print head, have a section-wise decreasing cross-section, the viscosity is reduced by the structure-viscous behaviour described under chapter 2.2. This, together with the heating of the print head, improves the flow behaviour from the feed cylinders to the dispensing needle at the print head.

The 3D printer is a modified Ender 5 Pro (Creality 3D Technology Co., Ltd, Shenzhen, China) with a Duet 3 6HC mainboard (Duet3D Ltd, Peterborough, UK). The main difference to a commercial 3D printer is the integration of the previously described feeding system, the modified print head and the heating lid for curing the individual printed silicone layers.
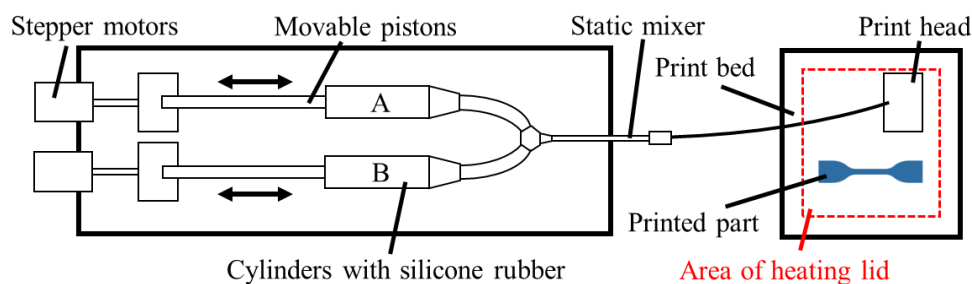

Figure 1. Sketch of the feed unit and the 3D printer

The Duet mainboard's extensive configuration options allow direct integration of all stepper motors and thus a freely adjustable mixing ratio of the silicone components. Furthermore, the silicone feeding can be interrupted via negative movement commands of the pistons, which enables a more precise dispensing. However, a comparable retraction as known from FDM printers is not possible. The temperatures of the print head and the print bed can be freely controlled. Another axis is mounted on the printer, which moves a heating lid in z-direction to bring it as close as possible to the last printed layer of the part. A heat gun supplies heated air via a heat-resistant hose to the part, accelerating the curing process so that the next layer can be printed after a short time. The heat gun is also controlled by

the mainboard. The recording of the system pressure at various measuring points is possible through an external monitoring system and takes place parallel to the printing process.

2.4. Print settings and test specimens

Preliminary tests indicated that certain parameters have to be set correctly for reliable printing results. Between the printed layers, the material must be cured for several seconds via the heating lid described above. This creates a solid base for the following layer. After each layer, the heating lid moves just above the part and stays there for 140 seconds at a temperature of 210 °C set on the heat gun. To reduce the viscosity and thus the system pressure, the print head is heated to 60 °C. The print bed is heated to 80 °C in order to accelerate the curing of the first layers. The layer height is 0.4 mm with a nozzle diameter of 0.84 mm. The overlap between the outer contour and the infill is 10%, which allows the silicone to adhere without creating faulty contours.

The geometry according to ISO 37 Type 1 is used for printing the tensile test specimens (see Figure 2). Tensile specimens from this standard are specially shaped to be able to test rubber-like materials in a suitable way. The parameters to be investigated are the printing speed and the infill angle. The printing speeds are 5, 10 and 15 mm/s. There is only one printed contour line, so the effect of the infill angle is stronger while still ensuring contour accuracy. Four pieces of each parameter variation of the test specimens are printed and then analysed.

In order to take into account the influence of controlled subsequent curing, four additional test specimens are printed and then cured for 4 hours at 200 °C in a laboratory oven. In addition, four test specimens are cast from the same material as a reference. These eight tensile specimens are also examined optically and mechanically.
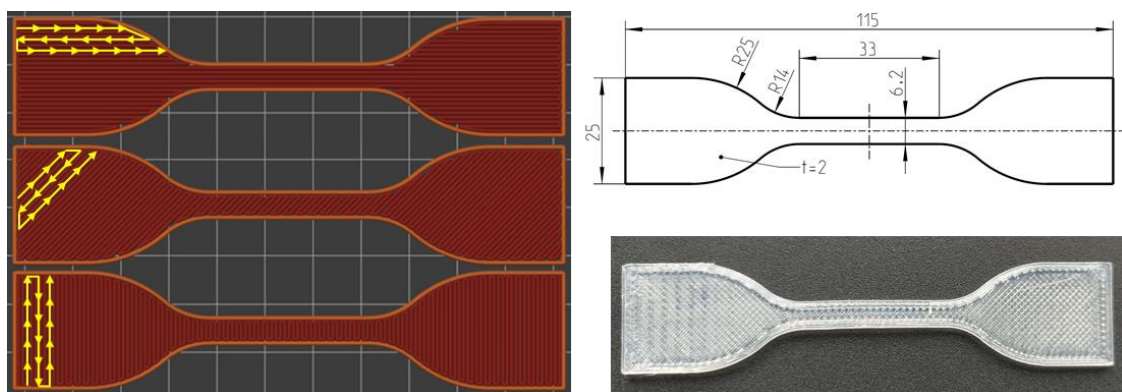

Figure 2. Infill angles of 0°, 45° and 90° (left), sketch of tensile specimen according to ISO 37 Type 1 (top right) and printed tensile specimen (bottom right)

2.5. Micro-CT analysis

Using a CT-ALPHA 240 micro-computer tomograph (ProCon X-Ray GmbH, Sarstedt, Germany), the test specimens are examined for air pockets in the base material, incomplete bonds between the printed layers and the real cross-section of the tensile specimens. The scans are performed with a filament and a target made of tungsten. A cathode voltage of 120 kV and 35 W radiation power are applied to the target. A detector with a pixel size of 100 µm is used. With 2500 individual images over 360°, a voxel size of 67.5 µm could be achieved. The evaluation was done with the software VGStudio 2022.4 (Volume Graphics GmbH, Heidelberg, Germany).

To measure the real, average cross-section of the narrowing on the tensile specimen, the volume of this partial area is measured over a length of 30 mm using the micro-CT scan images (see Figure 3). Divided by the length of the partial area, the relevant cross-section of the tensile specimen can be calculated. This cross-section is used to calculate the tensile strength of the respective tensile specimen. This compensates for any manufacturing tolerances that occur during the printing process.
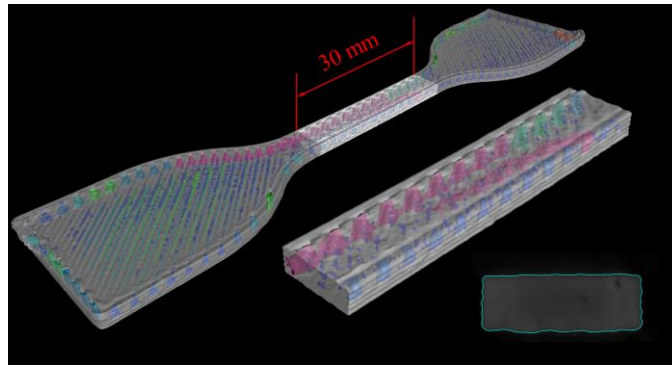
DESIGN FOR ADDITIVE MANUFACTURING

Figure 3. Relevant volume area and cross section of the tensile specimen analysed by micro-CT

2.6. Mechanical analysis

For comparison with the manufacturer's specifications on tensile strength and maximum elongation from Table 2, the tensile specimens described in section 2.4. are tested with a tensile testing machine inspekt solo M (Hegewald & Peschke Meß- und Prüftechnik GmbH, Nossen, Germany) for test forces up to 2.5 kN. Due to the transverse contraction during tensile stress, the test specimens tend to slip out of the clamping jaws. Therefore, the clamping supports 3D printed from PETG (Polyethylene Terephthalate Glycol) shown in Figure 4 are used. The measurement sequence is started by applying a pretension force of 5 N at a speed of 60 mm/s to the tensile specimen. After this pre-tensioning force has been reached, the actual measurement of the tensile force begins at a travel speed of 200 mm/s. Parallel to the force, the displacement is recorded until the tensile specimen breaks. As described in section 2.5., the real cross-section of the tensile specimen, captured by micro CT-scans, is used to calculate the tensile strength values. From these characteristics, the tensile strength and the elongation, related to the pre-tensioned length, of the tensile specimen can be calculated.
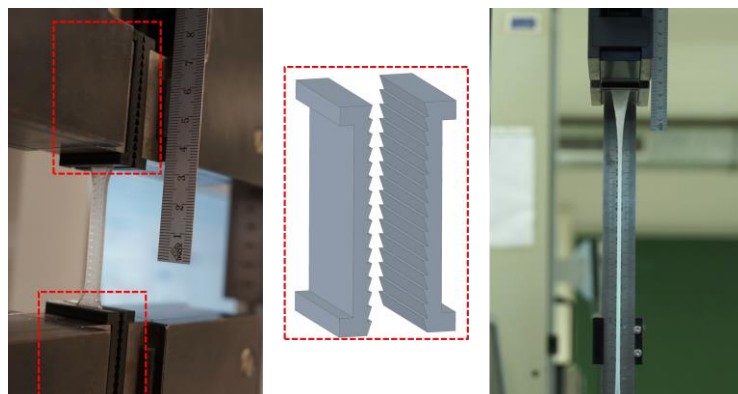

Figure 4. Clamped tensile test specimen; with and without load; using clamping supports

3. Results

For all tensile specimens described in section 2.4. the results of the micro-CT scans explained in section 2.5. and the tensile tests carried out afterwards in section 2.6. are presented below. In the micro-CT scans, the focus is on the air cavities within the test specimens. The tensile tests focus on the tensile strength and the maximum elongation.

The complete part volumes are used for the most meaningful recording of the cavities in relation to the printing speed and the infill angles. Due to the large volume of the individual tensile specimens compared to the partial volume in Figure 3, better statistical statements can be made regarding the air cavities.

As can be seen in Figure 5, only 23 of 36 tensile specimens broke in the relevant, tapered area (see Figure 3). The breakages in the false location resulted from air cavities and defects in the parts caused by the printing process. This is due to stress peaks through these cavities, which can be considered as

notches. For this reason, only the 23 tensile specimens that tore in the relevant area are used for the evaluation of the tensile strength. In addition, only the volumes, cross-sections and pore cavities in this 30 mm long area (see Figure 3) are evaluated in relation to the tensile strength.
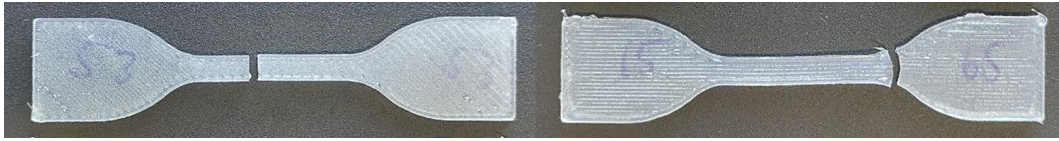

Figure 5. Tensile specimens with breaking location in the relevant test area (left) and outside; at the transition radius (right)

3.1. Micro-CT analysis for air cavities

Using CAD data, slicer calculations and micro-CT images, volume differences can be detected at different stages of the tensile specimen's fabrication. These are the following stages and volumes:

- Ideal geometry according to the dimensions in Figure 2, as shown in CAD, injection moulded or punched (Figure 6 left).
  - 3.653,82 mm³
- Sliced geometry, taking into account the layer and line structure of the part, resulting in slightly different volumes depending on the infill angle (Figure 6, center).
  - 0° = 3.600 mm³
  - 45° = 3.650 mm³
  - 90° = 3.670 mm³
- Micro-CT scanned geometry of the real tensile specimen. The air cavities in the part are shown multicoloured (Figure 6 right).
  - Different volumes for each part

As previously indicated by the slicer volumes, there is a theoretical volume difference of up to 2 % between the three selected infill angles. All other settings are the same as described in section 2.4.
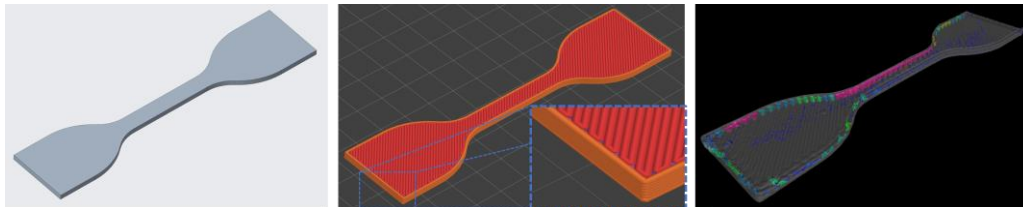

Figure 6. Comparison of the theoretical CAD volume of the tensile specimen (left), the target volume with 45° infill angle out of the Prusa Slicer (center) and the actual volume of the micro-CT scanned, 3D printed part with 45° infill angle (right)

Figure 7 shows an example of three micro-CT scans of 3D printed tensile specimens with the three different infill angles. It is also evident here that the tensile specimen with 0° infill angle (Figure 7 left) shows the smallest volume due to large air cavities between the layers. At an infill angle of 45° (Figure 7, center), larger air cavities can be seen in the outer zones of the tensile specimen. The infill angle of 90° (Figure 7 right) shows the smallest air cavities.
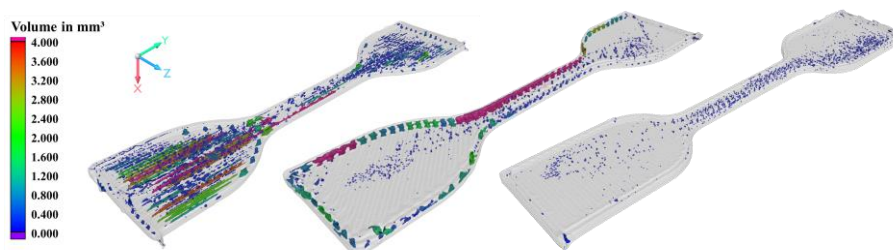

Figure 7. Micro-CT scans samples with infill angles of 0° (left), 45° (center) and 90° (right)

The results described above are confirmed by the evaluation of all tensile specimens. On the one hand, a trend can be seen on the left side of Figure 8, where the amount of air cavities decreases in percentage as the infill angle increases. On the right side of Figure 8, on the other hand, no correlation can be seen between the percentage of air cavities and the printing speed. The air cavity volume in these graphs refers to the entire test specimen volume.
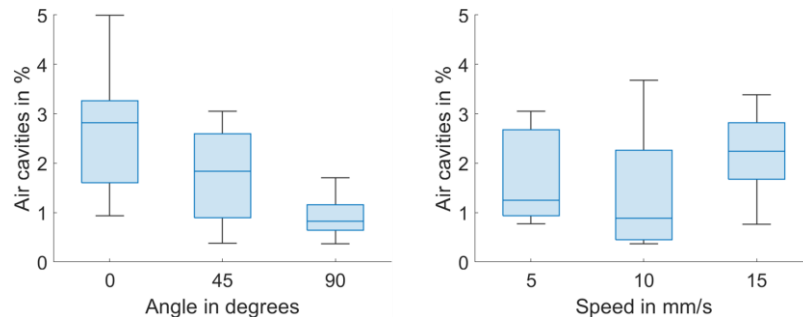

Figure 8. Percentage of air cavities in the volume of the entire tensile specimen related to the infill angle (left) and the printing speed (right)

3.2. Tensile strength of the test specimens

The graphs in Figure 9 show the relationships between the amount of air cavities, the infill angle and the printing speed to the real stress. With a low percentage of air cavities, a trend towards higher tensile strength can be seen. At the same time, a higher tensile strength can be seen at an infill angle of 45° than at 0°. The highest tensile strength is achieved at 90°. Again, analogous to the air cavity analysis in section 3.1, the printing speed has no significant influence on the tensile strength of the tensile specimens.
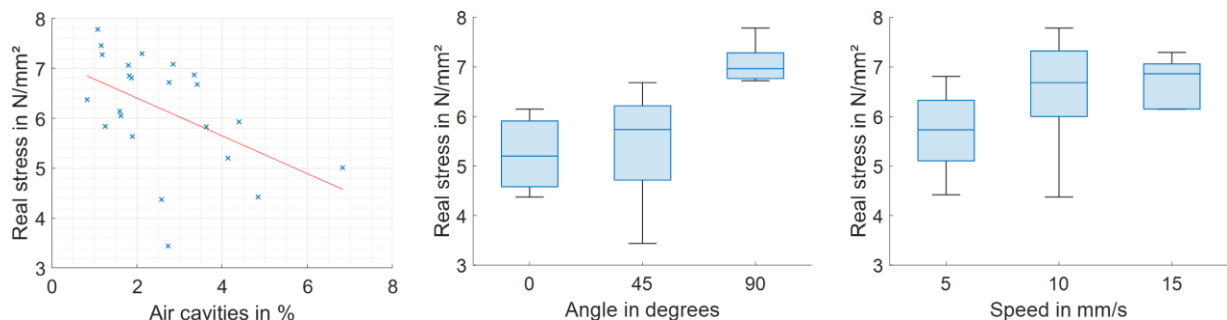

Figure 9. Real stress related to the relevant partial volume as a function of the air cavity volume (left), the infill angle (center) and the printing speed (right)

A distribution of the tensile strength of the relevant specimens in a range from 3.44 to 7.78 N/mm² can be seen. The highest tensile strength at an infill angle of 0° is 6.15 N/mm², at 45° it is 6.68 N/mm² and at 90° there is 7.78 N/mm².

Figure 10 shows representative stress-strain curves of four cast reference specimens, four printed specimens with additional curing at 200 °C for four hours after fabrication and one printed specimen for each infill angle.

The additively manufactured tensile specimens show a similar Young's modulus to the cast specimen, regardless of the infill angle. The post-cured tensile specimens have a higher Young's modulus but no higher tensile strength than the other specimens. As can be seen in Figures 9 and 10, a tensile specimen with an infill angle of 90° has a maximum tensile strength of 7.78 N/mm². The maximum tensile strength of the most robust cast specimens is 10.09 N/mm² (see Figure 10). The tensile strengths of the three other cast tensile specimens are in the same range. The supplier of the silicone Elastosil LR 3003/50 A/B states a maximum tensile strength of 10.3 N/mm² (see Table 2).
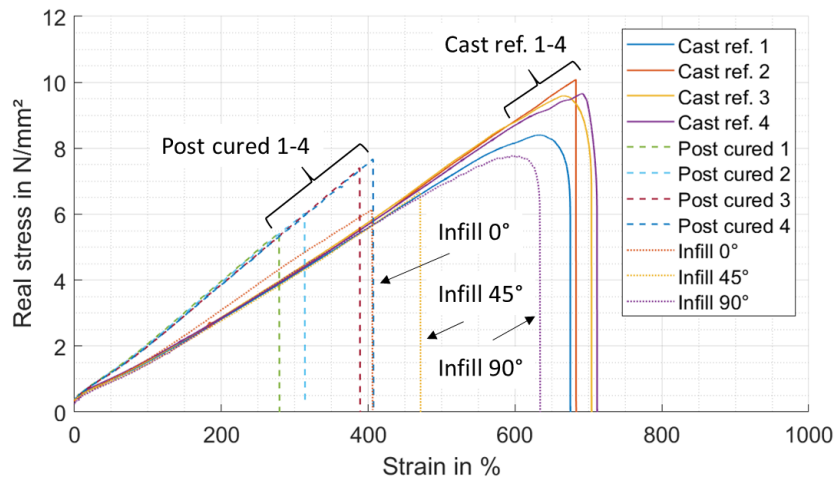
Figure 10. Stress-strain curves of four cast tensile specimen, four printed, post-cured tensile specimen and printed tensile specimens at 0˚, 45˚ and 90˚ infill angle

4. Discussion

4.1. Micro-CT analysis for air cavities

Comparisons of the theoretical and actual volumes under section 3.1. show a relationship between the air cavities and the infill angle. The volume differences calculated by the slicer for the test specimens manufactured according to ISO 37 Type 1 are confirmed by micro-CT images. More precisely, a trend can be observed in which the air cavity volume decreases with increasing infill angle. Since all other slicer settings are identical, other influences can be excluded.

As can be clearly seen in Figure 11, the largest air cavities occur in the transition area of the radii at an infill angle of 0°. With an infill angle of 45°, very few air cavities can be seen in the upper half of the radius transition area, but the largest in the lower half. With an infill angle of 90°, the fewest air cavities are created overall. The defects visible in the slicer are found very similarly in the printed tensile specimens. A spreading of the liquid layers during the printing process and thus an increased density of the parts is not visible. Therefore, the relationship between the infill angle and the air cavities is based purely on geometry, as it is not possible to achieve a finer resolution with the given nozzle diameter when approaching the shallow angles within the transition radii. Theoretically, these imperfections could be minimised by a larger overlap of the infill with the outer layer, but in practice this approach would worsen the printing process and the dimensional accuracy due to an over-extrusion of silicone. Similar effects have already been described by Agarwala et al. (1996) for the FDM process. With an infinitely small nozzle diameter, the infill angle would have, theoretically, no influence on the air cavity volume.
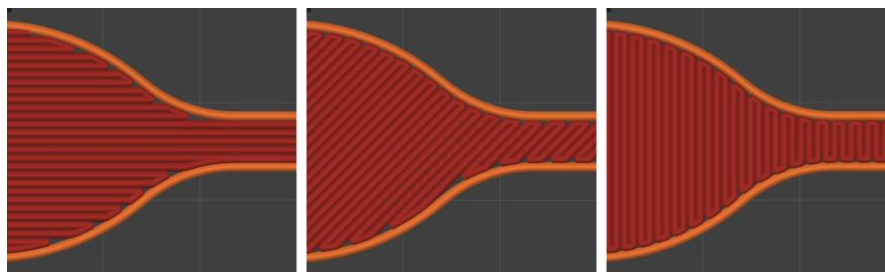

Figure 11. Visible differences of air cavities in the slicer between infill angles of 0˚ (left), 45˚ (center) and 90˚ (right)

4.2. Tensile strength of the test specimens

Based on the tests of own tensile specimens made by casting according to ISO 37 type 1 from the silicone Elastosil LR 3003/50 A/B, which is also used for the 3D printing application, a basic validity of the

tensile tests can be confirmed. With the maximum tensile strength of 10.09 N/mm² (see Figure 10, Cast ref. 2, orange line), the most robust cast test specimen achieves almost 98 % of the tensile strength of 10.3 N/mm² specified by the supplier (see Table 2).

The tensile strengths of the 23 tensile specimens torn in the relevant area (see Figures 3 and 5), related to the volumes of the air cavities and the infill angles, spread widely, as can be seen in Figure 9. This spread results from air cavities, which already exist during the filling of the feeding unit with the silicone. These air cavities are transported to the print head and then reappear in the printed part. This not only reduce the real cross-section of the tensile specimen, but also create notches in the part. As a result, there are stress peaks in the area of the air cavities. However, an increasing trend in tensile strength can be seen as the volume of the air cavities decreases and the infill angle increases. As described in section 4.1, there is a purely geometric relationship between the air cavity volume and the infill angle. This results in the highest tensile strength at an infill angle of 90°, as the volume, and thus also the cross-section and density, are highest in the relevant area of the tensile specimen.

These findings match the test results of Liu et al. (2023). In addition to fibre-reinforced tensile specimens made of silicone, they also tested unreinforced specimens. They also found that the amount of air cavities, and thus also the density of the tensile specimens, is related to the infill angle. A lower density results in a lower tensile strength. The anisotropy described for this reason is increased in the tensile specimens of Liu et al. (2023) by the large path widths and layer heights and the resulting rougher printing resolution.

Compared to the established, extensively investigated, FDM process with thermoplastic materials, the highest tensile strength with a perpendicular layer orientation to the pulling direction is, however, surprising. The anisotropic tensile strength behaviour of the layered parts normally results in increased tensile strengths along the pulling direction of the printed lines (Gibson et al., 2015). This is related to the incomplete fusing of the individual layers. In the case of the tensile specimens printed from silicone, the micro-CT scans reveal a better connection between the layers and lines and thus an almost isotropic structural behaviour in x-y plane. Tensile specimens orientated in the z axis could not be printed.

4.3. Comparison to existing design information for AM of silicon

According to the review by Liravi and Toyserkani (2018), there is a constant demand for research to collect design and process-specific parameters for the design of AM parts made of silicone and the necessary additive manufacturing systems. Luis et al. (2020) even suggest that an ASTM or similar standard for AM of silicones, in this case in the medical sector, is essential.

As outlined in section 1.2, scattered research results are available for a wide range of silicones and applications. Analogous to the findings in this paper, Liravi et al. (2015) and Martin et al. (2021) investigate printing speeds, Martin et al. (2021), Luis et al. (2020) and Liu et al. (2023) investigate temperatures of the printing bed, the nozzle or an additional hot air supply, and Martin et al. (2021) and Liu et al. (2023) investigate the layer orientation with regard to air cavities and the tensile strength of the parts. In all cases, however, lower viscosity silicones are used, as the resulting lower system pressures allow a more simple design of the AM system to be used. In addition to these results from other research institutes, the research field is extended by the information described in this publication on the additive processability of high-viscosity industrial silicones, which are not initially designed for use in AM.

5. Conclusion, design advice and outlook

This paper describes the additive manufacturing and analysis of tensile specimens made from highly viscous 2-component silicone, which is typically used in injection moulding applications. The material is applied layer by layer with the help of an in-house developed feeding and dispensing system, which applies the silicone with a heated dispensing needle onto a heated print bed. The test specimens are analysed optically by means of micro-CT scans and mechanically by means of tensile tests. In order to create a universal applicability, these experimental results are used to identify design and manufacturing parameters for AM machines and printed parts.

In order to ensure optimum feeding of the high-viscosity silicone to the print head, the structural viscous material behaviour was first analysed by means of rheological tests and then implemented in the design

of gradually narrowing feeding hose sections. Furthermore, it was possible to identify a correlation between the infill angle of the printed tensile specimens and the resulting air cavities through the micro-CT scans. The tensile tests revealed a further correlation between the amount of air cavities, and thus also the infill angle, and the tensile strength of the specimens. Good tensile strengths of the additively manufactured specimens could be achieved compared to the supplier's specifications and to reference tests with casted test specimens. Compared to additive manufacturing processes with thermoplastics, this results in a better connection of the layers and lines. This means that less attention needs to be paid to the alignment of the layers or the infill angle in relation to the load direction. More relevant seems to be the minimisation of any air cavities. The infill angle must therefore be selected for the part in the slicer in such a way that as few air cavities as possible are created.

Based on the results, future parts are created with regard to a minimum air cavity volume and optimised for production by means of the slicer. Adjustments to the line overlap, adapted curing temperatures and times of the individual layers as well as other infill patterns may be relevant here. The general part design no longer needs to include the consideration of anisotropy in the x-y plane, as is common with the FDM process. In addition, at least one other low-viscosity industrial silicone is to be investigated in the future with the existing system.

Acknowledgement

References

Agarwala, M.K., Jamalabad, V.R., Langrana, N.A., Safari, A., Whalen, P.J., et al. (1996), "Structural quality of parts processed by fused deposition", *Rapid Prototyping Journal*, Vol. 2 No. 4, pp. 4–19. https://doi.org/10.1108/13552549610732034

Gibson, I., Rosen, D. and Stucker, B. (2015), *Additive Manufacturing Technologies*, Springer New York, New York, NY. https://doi.org/10.1007/978-1-4939-2113-3

Leineweber, S., Reitz, B., Overmeyer, L., Sundermann, L., Klie, B. and Giese, U. (2022), Additive Manufacturing and Vulcanization of Natural and Synthetic Rubbers. *Logistics Journal: Proceedings*, Vol. 2022., Iss. 18 https://doi.org/10.2195/lj_proc_leineweber_de_202211_01

Liravi, F., Darleux, R. and Toyserkani, E. (2015), "Nozzle dispensing additive manufacturing of polysiloxane: dimensional control", *International Journal of Rapid Manufacturing*, Vol. 5 No. 1, p. 20. https://doi.org/10.1504/IJRAPIDM.2015.073546

Liravi, F. and Toyserkani, E. (2018), "Additive manufacturing of silicone structures: A review and prospective", *Additive Manufacturing*, Vol. 24, p. 232-242. https://doi.org/10.1016/j.addma.2018.10.002

Liu, W., Peeke, L.M., Periyasamy, M., Campbell, R.R. and Hickner, M.A. (2023), "Additive manufacturing of silicone composite structures with continuous carbon fiber reinforcement", *Polymer Engineering & Science*, Vol. 63 No. 6, pp. 1716–1724. https://doi.org/10.1002/pen.26318

Luis, E., Pan, H.M., Sing, S.L., Bajpai, R., Song, J., et al. (2020), "3D Direct Printing of Silicone Meniscus Implant Using a Novel Heat-Cured Extrusion-Based Printer", *Polymers*, Vol. 12 No. 5. https://doi.org/10.3390/polym12051031

Martin, S., Gugel, L., Martin, T., Preis, A., Reitelshöfer, S., et al. (2021), "Cost-efficient, true silicone printer with variable material spectrum for individualized medical applications", *Procedia CIRP*, Vol. 104, pp. 435–439. https://doi.org/10.1016/j.procir.2021.11.073

Plott, J. and Shih, A. (2017), "The extrusion-based additive manufacturing of moisture-cured silicone elastomer with minimal void for pneumatic actuators", *Additive Manufacturing*, Vol. 17, pp. 1–14. https://doi.org/10.1016/j.addma.2017.06.009

Wacker Chemie AG (2022), *ELASTOSIL® LR 3003/50 A/B Datasheet*. [online] Wacker Chemie AG. Available at: https://www.wacker.com/h/de-gb/medias/ELASTOSIL-LR-300350-AB-en-2022.06.17.pdf (accessed 06.10.2023).